atmosphere

Article

High Temporal Resolution Analyses with GOES-16 Atmospheric Motion Vectors of the Non-Rapid Intensification of Atlantic Pre-Bonnie (2022)

Russell L. Elsberry [1,2,*], Joel W. Feldmeier [2], Hway-Jen Chen [2], Christopher S. Velden [3] and Hsiao-Chung Tsai [4]

1 Lyda Hill Institute for Human Resilience, University of Colorado-Colorado Springs, Colorado Springs, CO 80918, USA
2 Department of Meteorology, Naval Postgraduate School, Monterey, CA 93943, USA
3 Madison Cooperative Institute for Meteorological Satellite Studies, University Wisconsin, Madison, WI 53706, USA
4 Department of Water Resources and Environmental Engineering, Tamkang University, New Taipei City 251301, Taiwan; hctsai@mail.tku.edu.tw
* Correspondence: relsberr@uccs.edu

Abstract: Four-dimensional COAMPS Dynamic Initialization (FCDI) analyses that include high-temporal- and high-spatial-resolution GOES-16 Atmospheric Motion Vector (AMV) datasets are utilized to understand and predict why pre-Bonnie (2022), designated as a Potential Tropical Cyclone (PTC 2), did not undergo rapid intensification (RI) while passing along the coast of Venezuela during late June 2022. A tropical cyclone lifecycle-prediction model based on the ECMWF ensemble indicated that no RI should be expected for the trifurcation southern cluster of tracks along the coast, similar to PTC 2, but would likely occur for two other track clusters farther offshore. Displaying the GOES-16 mesodomain AMVs in 50 mb layers illustrates the outflow burst domes associated with the PTC 2 circulation well. The FCDI analyses forced by thousands of AMVs every 15 min document the 13,910 m wind-mass field responses and the subsequent 540 m wind field adjustments in the PTC 2 circulation. The long-lasting outflow burst domes on both 28 June and 29 June were mainly to the north of PTC 2, and the 13,910 m FCDI analyses document conditions over the PTC 2 which were not favorable for an RI event. The 540 m FCDI analyses demonstrated that the intensity was likely less than 35 kt because of the PTC 2 interactions with land. The FCDI analyses and two model forecasts initialized from the FCDI analyses document how the PTC 2 moved offshore to become Tropical Storm Bonnie; however, they reveal another cyclonic circulation farther west along the Venezuelan coast that has some of the characteristics of a Caribbean False Alarm event.

Keywords: tropical cyclone non-rapid intensification; atmospheric motion vectors; dynamic initialization analyses; tropical cyclone track prediction; tropical cyclone outflow burst dome

check for updates

Citation: Elsberry, R.L.; Feldmeier, J.W.; Chen, H.-J.; Velden, C.S.; Tsai, H.-C. High Temporal Resolution Analyses with GOES-16 Atmospheric Motion Vectors of the Non-Rapid Intensification of Atlantic Pre-Bonnie (2022). *Atmosphere* **2024**, *15*, 353. https://doi.org/10.3390/atmos15030353

Academic Editors: Ching-Yuang Huang, Shu-Ya Chen and Kao-Shen Chung

Received: 17 January 2024
Revised: 11 March 2024
Accepted: 12 March 2024
Published: 14 March 2024

1. Introduction

The intensification, especially the rapid intensification (RI; 30 kt/day), of tropical cyclones (TCs) has been a central focus of forecasters and researchers for many years. Indeed, Rios-Berrios et al. (2024) [1] have provided a comprehensive (241 references) review of TC intensification and environmental vertical wind shear (VWS). Their focus was on the vertical tilt of the TC vortex, and they identified four pathways to TC intensification: (i) vortex tilt reduction; (ii) vortex reformation; (iii) axisymmetrization of precipitation; (iv) outflow blocking. Rios-Berrios et al. (see Figure 14 in [1]) summarize the key structural properties of intensifying TCs in moderate VWS versus non-intensifying TCs. An intensifying TC has a relatively small vortex tilt, nearly symmetric deep convection around the center, and relatively large air–sea fluxes. By contrast, a non-intensifying TC has a relatively large vortex tilt, highly asymmetric deep convection in the down-shear half of the vortex, but also relatively large air–sea fluxes in that down-shear half of the vortex. At least, for Atlantic TCs, the ingestion of dry air may disrupt the intensification either through radial ventilation, downward ventilation, or a combination of both.

The observational recommendation of Rios-Berrios et al. [1] is to utilize new-generation GOES satellites, small satellites, and uncrewed aircraft in addition to crewed research aircraft missions into early-stage TCs to increase our understanding of the intensification stage of both weak and mature TCs. An important objective of the Office of Naval Research Tropical Cyclone Rapid Intensification (TCRI) program has been to obtain aircraft observations in conjunction with the NOAA Hurricane Research Division (HRD) to better understand and predict RI events. During the 2022 season TCRI field experiment, the HRD team and the TCRI team would meet each morning to review the global and regional numerical model forecasts, searching for candidate circulations that might undergo RI within the flight range of the NOAA aircraft. In many RI situations following formation events, the aircraft would have to be deployed a day earlier from the base in Tampa/St. Petersburg, Florida, to a base in the eastern Caribbean. If three or more consecutive missions in the same circulation were anticipated, then the aircraft may have to be deployed two days in advance of the first mission to allow for a rest day before those three research missions started. In such a scenario, the HRD/TCRI planning meeting would need forecast guidance at least 3 days in advance of the first mission to alert the aircraft managers who require 24 h to prepare the aircraft for a deployment.

Such an opportunity existed on 24 June 2022, when a disturbance moved offshore from the western coast of North Africa (Papin 2022) [2]. This disturbance rapidly moved westward, and at 00 UTC on 28 June, the National Hurricane Center (NHC) issued an Advisory 1A. In that advisory, the Potential Tropical Cyclone (PTC 2) was at 8.8° N, 51.6° W, had a maximum wind speed of 35 kt, and had a 70%/90% probability of becoming a Tropical Storm (TS) within 48 h/120 h. Note that, although PTC 2 had a V_{max} of 35 kt, NHC did not call it a TS because the NHC definition of a TS requires a westerly wind on the equatorward side. Since PTC 2 was translating west–northwest at 16 kt in that first advisory, it would not be expected to have such a westerly wind component.

An experimental TC lifecycle-prediction model (Elsberry et al., 2022) [3] based on the ECMWF ensemble (ECEPS) was expected to be capable of providing the necessary early guidance as to the track, formation, and possible RI of the PTC 2 passing near Venezuela. This ECEPS-based lifecycle-prediction model had been very successful in providing earlier forecasts in the eastern North Pacific of the Time-to-Tropical Storm (T2TS) timing and position than were available from the NHC advisories. Elsberry et al. [3] also demonstrated that the ECEPS-based predictions were capable of forecasting the Time-to-Hurricane (T2HU) following the T2TS. These T2TS and T2HU times were provided to the nearest six-hour synoptic time along Weighted Mean Vector Motion (WMVM) track forecasts, in which the largest weight is given to the member track vectors that are the most similar to the WMVM vectors of the past 12 h.

In the ECEPS track prediction from 0000 UTC 24 June 2022 (Figure 1), the individual ensemble member track forecasts (grey lines) were tightly clustered about the WMVM track forecast (black dots at 48 h intervals) when the PTC 2 was in the eastern Atlantic. An important feature is that the PTC 2 disturbance was predicted to be rapidly translating from the eastern Atlantic all the way to Venezuela, which might be a factor in an RI forecast. Note also that there is a trifurcation (three clusters) of member track forecasts that began after PTC 2 was predicted to pass the north of Venezuela. The three clusters were defined based on the track latitudes upon crossing to the west of 110° W. Cluster 1 contains all tracks with latitudes ≤14° N, and the Cluster 2 tracks are between 14° N and 18° N. The Cluster 3 tracks are >18° N and these include all remaining ensemble member tracks that did not reach 110° W. Attention is especially drawn to the southern track cluster that was predicted to pass closest to the Venezuelan coast and later crossed Central America into the eastern North Pacific.

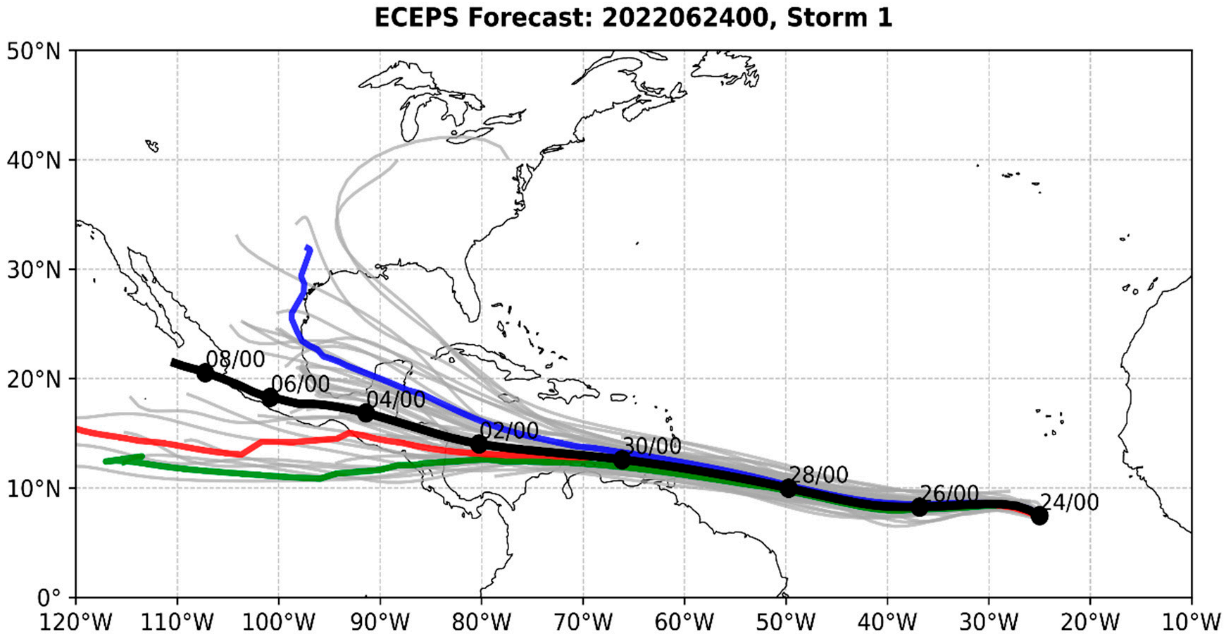

Figure 1. Weighted Mean Vector Motion (WMVM, black dots labeled with dates at 00 UTC) track forecast of PTC 2 from 0000 UTC 24 June 2022 using the ECEPS model, as described by Elsberry et al. [3]. Note that the ensemble member tracks tend to split into three track clusters after passing Venezuela, with the southern Cluster 1 in green, the middle Cluster 2 in red, and the northern Cluster 3 in blue.

The ECEPS WMVM track positions for Clusters 1, 2, and 3 from the 0000 UTC 24 June track forecast for the PTC 2 in Figure 1 are separately listed in columns 3–5 in Table 1, starting from 0000 UTC 28 June (Day 4.0). The deviations of those cluster track positions from the NHC track positions in column 2 are provided in bold numbers below the cluster track positions. Positive latitude deviations indicate northward errors and negative longitudinal deviations indicate eastward (slow translation) errors. Note that the southern Cluster 1 latitudinal errors in column 3 are only slightly (<1.0 degree) to the north of the NHC advisories until 12 UTC 1 July, when the PTC 2 track was well past Venezuela. The middle Cluster 2 track latitudinal errors in column 4 were only 0.4–0.7 degrees farther to the north than the Cluster 1 errors in column 3, until 00 UTC 2 July. By contrast, the northern Cluster 3 track latitudinal errors in column 5 were already 0.5 degrees farther north of the Cluster 1 error at 00 UTC 28 June (Day 4.0 in this 0000 UTC 24 June forecast). By 12 UTC 29 June, the additional northward error for Cluster 3 relative to Cluster 1 had increased to 1.0 degrees latitude. The additional error had increased to 2.1 degrees latitude by 1200 UTC 1 July, for a total error of +3.5 degrees latitude relative to the NHC advisories.

Elsberry et al. [3] describe how the ECEPS weighted mean intensities along the WMVM track forecasts can be estimated either directly from the Marchok (2021) [4] vortex tracker intensity output, or indirectly from the weighted mean Warm Core Magnitude (WCM) calculations. The WCM-based intensity estimates along the Cluster 1–3 WMVM tracks at the top of Table 1 are provided at 12 h intervals in columns 3–5 at the bottom of Table 1. These weighted mean WCM-based intensity estimates are considered to represent the symmetric vortex intensities, and do not include the translation speed that would add to (subtract from) the vortex wind speed on the poleward (equatorward) side. Thus, it is difficult to directly compare these WCM-based intensities with the NHC estimates.

Table 1. ECEPS forecasts from 00 UTC 24 June 2022 of the PTC 2 track (table at top) and intensity (kt, bottom table) from the ECEPS Warm Core Magnitude predictions (see text) for the Storm 1 track Clusters 1, 2, and 3 in Figure 1 versus from the National Hurricane Center (NHC) advisories in column 2. Track forecast differences from the NHC positions are indicated in columns 3–5 by bold numbers enclosed in parentheses. Twelve-hour longitudinal differences between NHC positions in column 2 are indicated in italics, where a 5.1 difference in row 2 would be ~500 km in 12 h.

TRACK (Lat/Long)				
TIME	**NHC**	**Cluster 1**	**Cluster 2**	**Cluster 3**
00 UTC 6/28	8.8° N, 52.0° W [+4.5°W]	9.7° N, 49.6° W (+0.9; −2.4)	10.1° N, 50.5° W (+1.3; −1.5)	10.2° N, 49.6° W (+1.4; −2.4)
12 UTC 6/28	9.6° N, 56.5° W [+4.7° W]	10.3° N, 54.0° W (+0.7; −2.5)	10.8° N, 54.4° W (+1.2; −2.1)	11.1° N, 53.4° W (+1.5; −3.2)
00 UTC 6/29	10.6° N, 61.2° W [+5.1° W]	11.0° N, 58.2° W (+0.4; −3.0)	11.5° N, 58.5° W (+0.9; −2.7)	11.8° N, 57.4° W (+1.2; −3.6)
12 UTC 6/29	11.3° N, 66.3° W [+3.4° W]	11.5° N, 62.5° W (+0.2; −3.8)	12.2° N, 62.8° W (+0.9; −3.5)	12.5° N, 61.4° W (+1.2; −4.9)
00 UTC 6/30	11.9° N, 69.7° W [+3.4° W]	12.0° N, 66.8° W (+0.1; −2.9)	12.6° N, 67.0° W (+0.7; −2.7)	13.1° N, 65.3° W (+1.2; −4.4)
12 UTC 6/30	12.0° N, 73.1° W [+3.4° W]	12.3° N, 71.4° W (+0.3; −1.7)	12.8° N, 71.2° W (+0.8; −1.9)	13.6° N, 68.9° W (+1.6; −4.8)
00 UTC 7/1	11.9° N, 76.8° W [+3.7° W]	12.4° N, 75.7° W (+0.5; −1.1)	13.0° N, 74.9° W (+1.1; −1.9)	14.1° N, 72.2° W (+2.2; −4.6)
12 UTC 7/1	11.2° N, 80.3° W [+3.5° W]	12.6° N, 79.6° W (+1.4; −0.7)	13.0° N, 78.6° W (+1.8; −1.7)	14.7° N, 75.2° W (+3.5; −5.1)
00 UTC 7/2	10.9° N, 83.2° W [+2.6° W]	12.4° N, 82.7° W (+1.5, −0.5)	13.2° N, 81.8° W (+2.3; −1.4)	15.4° N, 77.9° W (+4.5; −5.3)
12 UTC 7/2	11.2 N, 85.8° W [+3.1° W]	12.2° N; 85.7° W (+1.0; −0.1)	13.6° N, 84.9° W (+2.4; −0.9)	16.3° N, 80.6° W (+5.1; −5.2)
INTENSITY (KT)				
	NHC	**Cluster 1**	**Cluster 2**	**Cluster 3**
00 UTC 6/28	35	26	29	31
12 UTC 6/28	35	26	31	39
00 UTC 6/29	35	28	42	45
12 UTC 6/29	35	26	39	52
00 UTC 6/30	35	34	58	74
12 UTC 6/30	35	34	48	68
00 UTC 7/1	35	38	65	91
12 UTC 7/1	35	60	75	97
00 UTC 7/2	45	48	75	103
12 UTC 7/2	35	41	81	114

In the case of Cluster 1 (column 3 in Table 1), the predicted vortex intensities were 26–28 kt during the first two days, 34–38 kt for a 36 h period, and then a rapid increase by 22 kt in 12 h to 60 kt. While this increase implies an RI event, it did not occur until the Cluster 1 circulation was about to make landfall in Central America. Cluster 2 intensity in column 4 was 29 kt at 0000 UTC 28 June (Day 4.0) and irregularly increased to 39 kt in 48 h. More regular intensifications of 17–20 kt in 24 h alternated with decays until 65 kt was predicted at 0000 UTC 1 July, and the peak intensity of 75 kt occurred when PTC 2 (now TS Bonnie) was still in the Caribbean Sea. Cluster 3 intensification was steadier from 0000 UTC 28 June (Day 4.0), starting at 31 kt and increasing to 74 kt at 0000 UTC 30 June (Day 6.0). After a slight decay to 68 kt at 1200 UTC 30 June, the Cluster 3 intensification continued to 114 kt at 1200 UTC 2 July because it continued to move over warm water in the western Caribbean.

In summary, the ECEPS forecast from 00 UTC 24 June indicated that a disturbance in the eastern Atlantic would approach the southern Caribbean on Day 5 and thus be within the range of the NOAA research aircraft. The track uncertainty also increased around Day 5 with a track trifurcation. If the southern track Cluster 1 gave a verification, then the ECEPS would predict that there would be no RI event while passing north of Venezuela, and the TCRI/HRD team need not deploy the NOAA research aircraft for the PTC 2. If the middle track Cluster 2 (slightly farther to the north) gave a verification, then the ECEPS would predict the likelihood of an RI event following the formation (Table 1, column 4). If this were true, then the TCI/HRD should be planning for missions as soon as the PTC 2 were within range in order to obtain observations prior to the formation, which was predicted to be at 00 UTC 29 June (Day 5.0).

The primary objective of this study is to demonstrate that FCDI analyses with the CIMSS high-density GOES-16 AMV datasets can be utilized to better understand why the PTC 2 did not undergo RI as it passed north of the coast of Venezuela. The NOAA research aircrafts were deployed but were not able to acquire the necessary datasets over Venezuela, or even very near the coast, due to flight restrictions. The high-resolution FCDI analyses are also utilized to diagnose intensity changes with more precision than the constant intensity of 35 kt, as indicated in the NHC Advisories 1–16 every six hours from 0000 UTC 28 June to 1200 UTC 1 July (column 2, lower Table 1). The FCDI analyses and COAMPS-TC (Doyle et al., 2014) [5] forecasts are also examined to determine whether the PTC 2 might become a Caribbean False Alarm (FA) circulation, as defined by Elsberry et al. (2014) [6]. If so, then the FCDI analyses allow the diagnosis of the vortex and environmental conditions, leading to these FAs that later may become TCs in the eastern North Pacific. In addition, these FCDI analyses are utilized as the initial conditions for two COAMPS-TC forecasts of the passage of PTC 2 along the coast of Venezuela. A summary and discussion will be presented in Section 5.

2. Data and Methods

2.1. Background on Newly Available Satellite-Derived AMV Datasets and FCDI Analyses

Elsberry et al. (2020a) [7] describe in detail the development of the FCDI technique that is capable of assimilating high-spatial- and high-temporal-resolution GOES-16 atmospheric motion vector (AMV) datasets. In addition to the routine GOES-16 full-disk multispectral image scan every 10 min and the Continental U.S. scanning every 5 min, the GOES-16 mesoscale scan mode allows one-minute imaging that can be targeted to follow a TC center within a 10° latitude by 10° longitude domain. Using this one-minute imagery, a research team at the University of Wisconsin Cooperative Institute for Meteorological Satellite Studies (CIMSS) has developed and refined automated algorithms to produce very-high-spatial-resolution AMVs, which greatly enhance the AMV coverage to resolve the small scales of the flow fields over the TC inner core and its surrounding environment (Stettner et al., 2019) [8].

The data assimilation challenge is to ingest these extremely high spatial density AMVs every 15 min (chosen dataset processing interval for TC case studies) and retain their information to continuously monitor the rapid evolution of the three-dimensional vortex structure and the associated intensity changes. Basically, every 15 min, a three-dimensional field of AMVs minus the COAMPS-TC model wind increments are nudged into the FCDI analysis model solution for the next 15 min until a new AMV dataset becomes available. The COAMPS model utilized in the FCDI analysis is triply nested. The fixed outer Domain 1 has 361 grid points east–west and 191 grid points north–south, with a grid spacing of 36 km. Domain 2 (Domain 3) has 367 (556) grid points east–west and 331 (556) grid points north–south, with a grid spacing of 12 km (4 km). Consequently, the entire GOES-16 meso-scan AMVs domain is contained within Domain 3 of the FCDI analyses, with a grid spacing of 4 km.

In addition to describing the fundamentals of the FCDI technique, that allow it to be a time-efficient dynamic initialization capable of incorporating more than 10,000 AMVs every 15 min, Elsberry et al. (Section 2.1.3 of [7] and their Appendix) introduced a near-surface wind field adjustment that acts as a low-level constraint on the distribution of deep convection relative to the translating center. In that Hurricane Irma data assimilation application presented by Elsberry et al. [7], the surface wind adjustment domain was translated every 15 min along a target pathway when a new AMV dataset became available. Each 6 h target pathway is simply a straight line from the t = 0 h of the assimilation cycle to the known 6 h ending position. The success of this surface wind field adjustment is that the FCDI analysis center at t + 6 h is predicted to be within fix uncertainty, relative to the next warning position. Thus, the next 6 h assimilation cycle then simply begins from that previous t + 6 h assimilation position with the three-dimensional variable fields. Consequently, no vortex relocation or introduction of a bogus vortex at the warning position is required as in a cold-start process. Furthermore, the FCDI analysis in the next 6 h assimilation cycle continues smoothly with no adjustments or re-balancing in the wind field or in the mass field.

2.2. Additional Documentations of the Enhanced AMV Datasets and FCDI Analyses

The importance of higher-frequency GOES-East AMVs for understanding and forecasting RI events during the lifecycle of Hurricane Joaquin (2015) was demonstrated by Elsberry et al. (2020b) [9]. Berg et al. (2016) [10] presented the official National Hurricane Center (NHC) report on Hurricane Joaquin. The AMV team at CIMSS provided their vertical wind shear (VWS-C) product that was based on reprocessed GOES-East AMVs at 15 min intervals (Hendricks et al., 2018) [11], and they presented the CIMSS Satellite Consensus (Velden and Herndon, 2020) [12] intensity changes at 30 min intervals. Elsberry et al. [9] first demonstrated that, over the entire lifecycle of Hurricane Joaquin, the linear correlation of the VWS-C with the SATCON intensity changes was −0.36 with substantial intensity increases (decreases) during negative (positive) VWS-C deviations from a moderate value of 8 m s^{-1}. During the first extreme RI event of 12 kt (6 $h)^{-1}$ between 1900 UTC and 2100 UTC 23 September 2015, the VWS-C correlation was −1.0. However, during a second longer RI event with an average rate of 7.4 kt (6 $h)^{-1}$ between 2100 UTC 2 October and 0900 UTC 3 October, the correlation with the VWS-C deviations was a positive 1.0. It is emphasized that these RI events during the Hurricane Joaquin (2015) lifecycle did not necessarily begin or end at the normal synoptic times (00, 06, 12, and 18 UTC) that are typically used in RI studies. Thus, one advantage of our FCDI analyses with the 15 min AMV datasets is the capability to define the non-synoptic starting and ending times of RI events. While RI events occur over multiple consecutive synoptic times, some events may nevertheless be missed without considering higher temporal resolutions.

In addition to the documentation of the new FCDI technique, Elsberry et al. [7] analyzed at 15 min intervals and predicted an RI event in Hurricane Irma (2017). Cangialosi et al. (2018) [13] presented the official National Hurricane Center (NHC) report on Hurricane Irma, which was one of the strongest and costliest hurricanes on record in the Atlantic basin. The distinguishing features of the Irma intensification were first an extreme RI period, an intermediate constant intensity period, and then a slower RI period. Only the COAMPS-TC forecast, initiated from an FCDI analysis that included the 15 min GOES-16 AMV dataset, accurately predicted the timing and persistence of the constant intensity period, and then resumed the deepening of Irma at the correct time and with an accurate rate of deepening. Elsberry et al. [7] demonstrated the FCDI analysis that was used, as initial conditions had a stronger outflow toward the northeast that had pushed a northerly environmental flow back to the east. The COAMPS 24 h forecast then had a stronger outflow in all quadrants that established what we refer to as direct connections with the adjacent synoptic circulations to the northeast and to the northwest that are considered favorable for sustained RI events.

Elsberry et al. [7] also examined the Hurricane Weather Research Forecast (HWRF) initialization (Lewis et al., 2020) [14], that included the same CIMSS high-density GOES-16 AMV datasets that were utilized in the FCDI analyses. Due to the sophisticated HWRF vortex initialization procedure, the high-density AMV HWRF initial analysis exactly matched the NHC best-track Minimum Sea-Level Pressure (MSLP) value at the initial time of 1800 UTC 3 September. However, the HWRF model forecast then rapidly deepened the MSLP by 15 mb in 12 h and by more than 25 mb in 24 h, and continued that rapid deepening right through the constant MSLP period. It is noteworthy that the HWRF model outflow magnitudes and horizontal areal extents remained small during this rapid deepening. While this is just one example, the rapid deepening in the high-density AMV HWRF forecast evidently occurs via a different mode than in the FCDI-based COAMPS-TC forecasts, in which sustained outflow bursts lead to the establishment of direct connections with the adjacent synoptic flows.

Elsberry et al. (2023a) [15] have also incorporated CIMSS high-temporal- and high-spatial-resolution GOES-16 AMV datasets into the FCDI to examine the Tropical Storm (TS) Henri case, that was another aircraft mission objective of the TCRI project. The first important result in Elsberry et al.'s study [15] was that the continuous FCDI analyses revealed that Henri was a subtropical cyclone with an intensity of ~20–25 m s^{-1} (40–50 kt) rather than a TS of 55–60 kt as in the NHC best track (Pasch et al., 2021) [16]. That is, the continuous FCDI 300 m wind vector analyses reveal highly asymmetric wind fields with near-zero wind speeds, about 150 km to the southwest of the center, and 15 m s^{-1} winds extending more than 300 km to the north–northeast of the center. While the horseshoe-shaped isotach maximum was >21 m s^{-1}, it was about 75 km from the center. These two characteristics are consistent with the NHC definition of a subtropical cyclone: *"a radius of maximum winds occurring relatively far from the center (usually greater than 60 n mi), and generally have a less symmetric wind field."*

The most important result presented by Elsberry et al. in [15] was the discovery in the continuous FCDI analyses of a rapidly intensifying mesovortex about 150 km to the south of the main Henri vortex, which occurred at the same time as that main vortex was decreasing in intensity in the FCDI analysis. This southern mesovortex had also expanded and intensified just as it approached the prior westward path of the main vortex. The FCDI analyses at 13,910 m document that, during that time, there were continually radial outflow vectors from that southern mesovortex that were passing over the region of the main Henri vortex to the north, which is consistent with its decay in time rather than undergoing RI as predicted by the regional numerical models [15].

Given that the southern Cluster 1 track close to the coast in Figure 1 did not have an RI event, and the above examples of OBDs in the FCDI analyses can distinguish RI events, the non-RI event hypothesis for pre-Bonnie was due to unfavorable land interaction plus the absence of sustained OBDs, that were directly connected to adjacent synoptic circulations.

3. Continuous FCDI Analyses of PTC 2

In this section, the continuous FCDI analyses forced with the high-density GOES-16 AMV datasets every 15 min will be examined in relation to the PTC 2 disturbance intensity changes during 0000 UTC 28. The procedures to create these continuous (15 min) FCDI analyses are described in Elsberry et al. [15]. The higher-spatial- and higher-temporal-resolution GOES-16 AMV datasets were available from 1800 UTC 27 June, which is 48 h before the first Cluster 2 RI event described above. The first NOAA research aircraft mission (NOAA 20220627 H1; https://nhc.noaa.gov/archive/recon/2022; accessed on 10 January 2024) was centered at that time, which provided flight-level winds, drop wind sondes, and Doppler radar for the COAMPS-TC model cold-start initial conditions for the FCDI analyses.

As described in Elsberry et al. [7,15], the FCDI analyses include a surface wind adjustment that constrains the low-level center to move along a target pathway toward the next six-hour NHC Working Best-Track (WBT) position. Due to the success of that surface wind adjustment to bring the low-level center at T + 6.0 h to within fix position uncertainty, the subsequent continuous FCDI analyses are warm starts from the previous t + 6.0 h three-dimensional fields of wind, pressure, temperature, and humidity fields of the FCDI analysis. As mentioned in Section 2, no insertion of a bogus vortex or dynamic re-balancing of the wind or mass fields are required in order to match either the MSLP or the Vmax. Rather, the continuous FCDI near-surface wind speed analyses occur in response to the COAMPS model adjustments to the constraints of the 15 min GOES-16 AMV datasets and to the surface wind adjustments.

3.1. June 28 AMV Datasets and FCDI Analyses

Some of the GOES-16 AMV datasets in three-hour increments between 0900 UTC 28 June and 1800 UTC 28 June that have been utilized in the continuous FCDI analyses are provided in Figure 2a–d. Our primary objective in utilizing the high-temporal- and high-spatial-resolution GOES-16 AMV datasets to construct outflow burst dome(s) is to depict the origin(s) and spreading of the outflow relative to the storm of interest. After some experimentation, yellow wind vectors for AMVs above 100 mb have been selected to identify where strong, deep convection associated with long-lasting mesoscale convective systems have originated, because those are the locations of strong diabatic heating in the column. If co-located with the low-level circulation center, that diabatic heating will contribute to mean sea-level pressure falls and spin-up of the low-level circulation into a possible RI event. If not co-located with the low-level circulation, the yellow vectors indicate the top of the adjacent OBD as it spreads out horizontally. While the OBD top slowly descends due to long-wave radiative cooling, the outflowing mass eventually reaches the leading edge, when more rapid subsidence occurs. This leading edge is first indicated by yellow vectors becoming red vectors (below 100 mb), and then by red vectors more rapidly becoming green vectors (below 150 mb). In fan-shaped OBD tops, the outflowing mass is horizontally spreading in both down-shear and across-shear directions. Alternating regions of yellow and red down-shear vectors indicate horizontal waves on the tp of the OBD. Red vector streaks in the yellow vector areas indicate where the across-shear spreading has opened gaps where those red vectors (below 100 mb) then become visible. If an OBD of an adjacent circulation encounters the target storm circulation outflow, it may be deflected around that target storm outflow. However, a stronger outflow from the adjacent OBD may shear off the top (warm core) of the target storm.

In Figure 2, the surface position of the PTC 2 disturbance is indicated by the asterisk near the center of each panel. These PTC 2 positions are interpolated at 15 min intervals between the six-hourly WBT positions. Note that the PTC 2 had strong aloft easterlies, as indicated by yellow AMVs with elevations above 100 mb (thinned to 1:10). While other data assimilation techniques generally require thinning of high-density AMVs, our FCDI utilizes every AMV that passes the quality-control rules. The outflow burst domes (OBDs) are not symmetric about their origin due to these strong easterlies. Rather, the OBDs are fan-shaped downstream of their origin, which is clearest in Figure 2b. Note that the red arrows (100–150 mb), emanating in all directions from an open area (ascent region) near 11° N, 57° W, are spreading downstream. In the west–northwest and west–southwest regions especially, yellow vectors above 100 mb indicate the warm outflow is buoyant and the top of the dome is still rising. The leading edge of the OBD in Figure 2b is depicted by very dense red vectors transitioning to very dense green vectors, which indicates that the OBD has spread out in a horizontal layer between 100 mb and 200 mb. Note also in Figure 2b that a portion of the OBD has swept over the location of PTC 2 near 9.5° N, 56.6° W, and the outflow leading edge is well to the south of PTC 2 near 8.7° N.

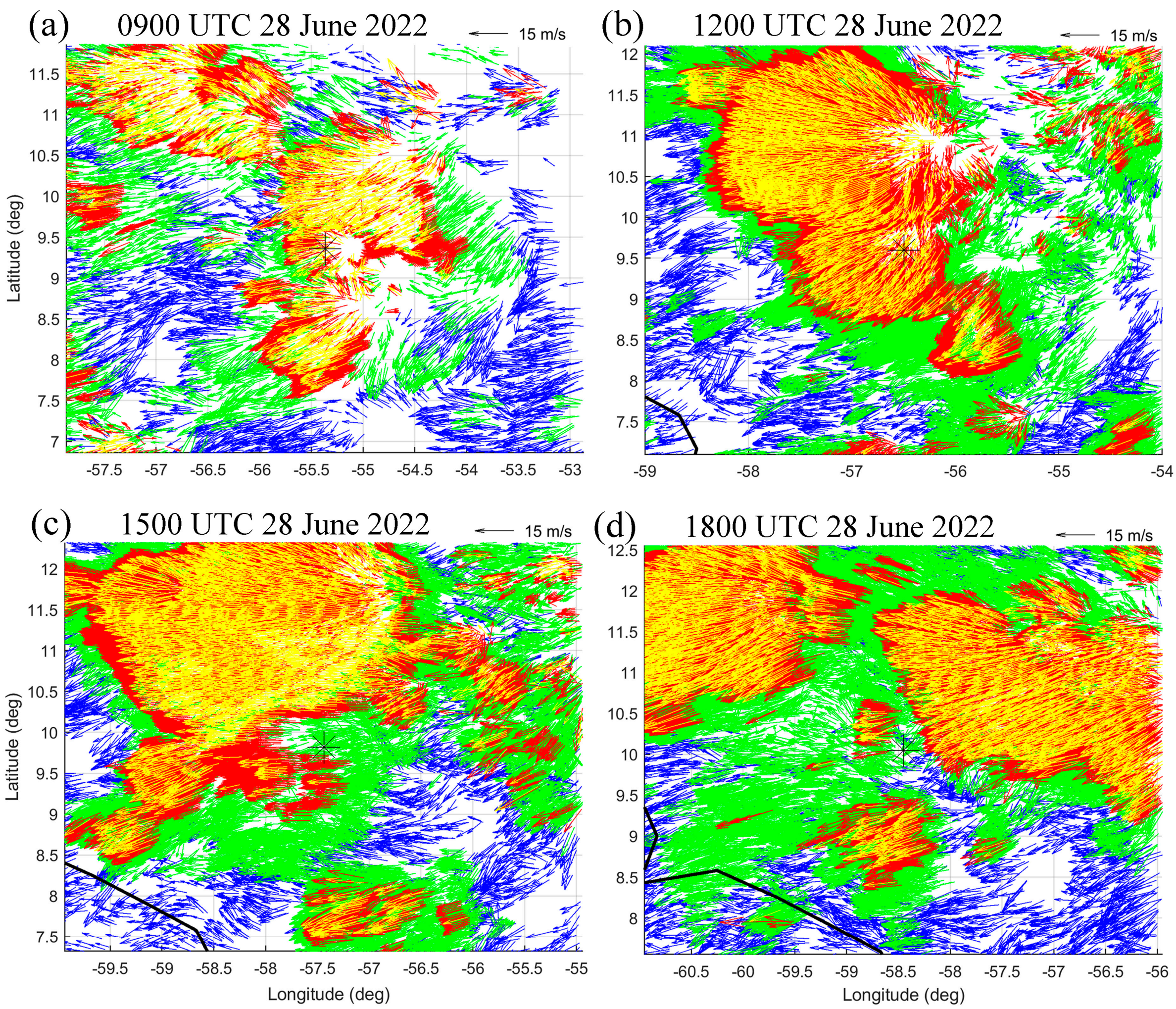

Figure 2. GOES-16 Atmospheric Motion Vectors (AMVs) reprocessed at 15 min intervals by CIMSS with yellow vectors above 100 mb, red between 100 and 150 mb, green between 150 and 200 mb, and blue between 200 and 250 mb, and centered on the near-surface positions of PTC 2 (asterisk) at (**a**) 0900 UTC 28 June 2022, (**b**) 1200 UTC 28 June, (**c**) 1500 UTC 28 June, and (**d**) 1800 UTC 28 June. The coastline of South America is indicated by black lines at bottoms of panels (**b**–**d**).

Three OBDs that may be affecting the PTC 2 disturbance are evident in Figure 2a. The largest OBD originates near 10.5° N, 54.6 W and mainly spreads toward the southwest, although the flow vectors on the equatorward side turn anticyclonically to become easterlies to the north of the PTC 2. A small OBD center is evident near 9.3° N, 55° 2 W just to the east of the PTC 2 position. It is likely that the PTC 2 OBD, which has enhanced easterlies on the west side and has enhanced southwesterlies on the east side, has been able to oppose an oncoming outflow stream associated with the first OBD to the north. The third OBD in Figure 2a is to the south of the PTC 2 with a fairly well defined center near 8.7° N, 55° W. While this third OBD has a small south–southeasterly branch toward the PTC 2, its primary outflow is toward the southwest.

Just three hours later (Figure 2b), the northern OBD has intensified and spread rapidly toward the west where it has apparently merged with a separate OBD in the 0900 UTC 28 June AMV plot (Figure 2a). As indicated above, the result is a large fan-shaped OBD covering most of the northwest section of the GOES-16 mesodomain. Note that, along the western leading edge, dense red (100–150 mb) AMVs are at the end of yellow (above 100 mb) AMVs and then transition to a narrow zone of green (150–200 mb) AMVs; this again indicates the rapidly descending air parcels on the leading edge of the OBD. Furthermore, there is a lobe of this northern OBD that is streaming toward the southwest and is expected to flow over the PTC 2 disturbance. Consequently, there is a layer between 100 and 200 mb of strong environmental flow that would soon be imposing vertical wind shear, which will likely weaken the PTC 2.

At 1500 UTC (Figure 2c), the major northern OBD has expanded to the north, to the west, and to the southwest. An interesting feature of the westward extension of the OBD is a long line of alternating yellow (above 100 mb) and red (100–150 mb) AMVs that may indicate gravity waves. Although not as distinct, there are also alternating yellow and red AMVs along the southwestward OBD. Note that there are now no yellow or red AMVs over the PTC 2. Rather, there are green (150–200 mb) AMVs flowing over the PTC 2 position, which suggests that the deep convection associated with the PTC 2 disturbance does not extend up to that layer at 1500 UTC.

Just three hours later (Figure 2d), the northern OBD translated farther to the west. Another extensive OBD with yellow (above 100 mb) and red (100–150 mb) AMVs is now present to the northeast of the PTC 2 disturbance. With only green (150–200 mb) AMVs over the PTC 2, it is expected that this new OBD will also spread over PTC 2 and continue to inhibit development of PTC 2. Indeed, the NOAA 202206228 H1 mission centered on 18 UTC 28 June (https://nhc.noaa.gov/archive/recon/2022/; accessed on 10 January 2024) did not find a closed PTC 2 circulation at flight level.

The reason that these 15 min AMV datasets have been presented in three-hourly intervals (rather than six-hourly synoptic times) is to convey how rapidly the OBDs developed and evolved relative to the PTC 2 during 28 June. Recall that the 15 min AMV datasets have been continuously inserted into the FCDI analyses since the cold-start initial conditions at 18 UTC 27 June. A series of FCDI wind analyses at 13,910 m at the same three-hourly intervals during 28 June is presented in Figure 3 to illustrate how these FCDI analyses have represented the OBDs described above. This 13,910 m elevation has been selected because the desire is to represent the tops of the OBDs. It is emphasized that the nudging term in the FCDI analysis is the difference between the AMV wind components at the AMV elevation—not necessarily at the 13,910 m FCDI wind components in Figure 3. The AMV nudging term effectively spreads AMV increments over the COAMPS layer depths in which they are applied. Finally, the FCDI analyses are here displayed in the larger COAMPS Domain 2 to show the OBD direct connections with adjacent synoptic circulations, which Elsberry et al. [15] demonstrated was a critical aspect of long-lasting RI event in the subtropical cyclone Henri (2021) event.

The advantage of the continuous FCDI analyses that incorporate the 15 min GOES-16 AMV datasets is the COAMPS model integrations in the FCDI adjust the interior three-dimensional wind, pressure, temperature, and humidity fields to those AMV nudging increments. The FCDI wind vector fields at 540 m are provided in Figure 4 to address the question of whether the PTC 2 intensity was constant at 35 kt during 28 June; if not, why not? An FCDI level near 500 m is selected as some of the NOAA P-3 aircraft observations were at that level. Six-hour synoptic times of 06 UTC, 12 UTC, and 18 UTC 28 June, and 00 UTC 29 June are examined for comparison with the NHC Advisories.

At 0900 UTC 28 June (Figure 3a), the 13,910 m FCDI analysis has a good representation of the dominant northern OBD in Figure 2a. While the GOES-16 AMVs in Figure 2a define two OBDs in the northern domain, these two OBDs are combined with a fan-shaped isotach maximum exceeding 24 m s^{-1}. Note that there is direct connection between 55° W and 56 W° of this OBD, with an adjacent synoptic circulation to the north beyond Domain 2. The AMV OBD toward the southwest just to the north of the PTC 2 (black dot in Figure 3a) appears to be much stronger than the ~12 m s^{-1} wind vectors in the FCDI analysis, which may indicate that that the AMV OBD is new and the FCDI analysis has not had time to respond. Similarly, the AMV OBD just to the east of the PTC 2 in Figure 2a is better organized and more intense than the burst in the FCDI analysis in Figure 3a. A similar comment applies to the third AMV OBD to the southeast of the PTC 2 in Figure 2a. The tentative explanation for these second and third AMV OBDs is that they are so recently developed that the FCDI analysis has not yet fully responded.

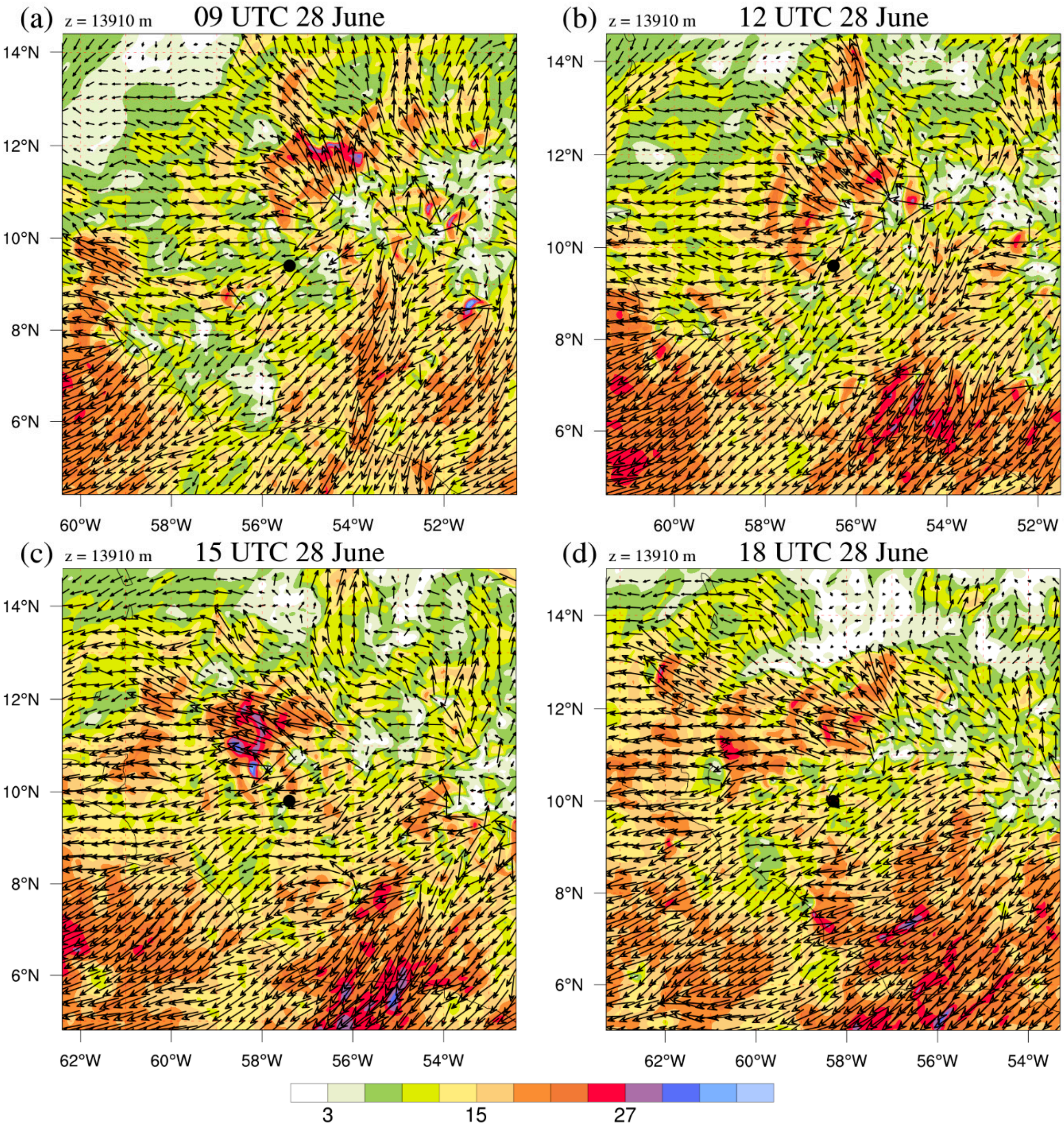

Figure 3. Wind vectors (m s^{-1}, isotach color scale at bottom) at 13,910 m relative to the PTC 2 disturbance (black dot) from continuous FCDI analyses that have incorporated 15 min GOES-16 AMV datasets from 1800 UTC 27 June through (**a**) 0900 UTC, (**b**) 1200 UTC, (**c**) 1500 UTC, and (**d**) 1800 UTC 28 June 2022.

Just as there was a large expansion in the AMV fan-shaped OBD to the west at 1200 UTC 28 June in Figure 2b, the 13,910 m FCDI analysis in Figure 3b has a similarly shaped outflow, with the leading edge of the isotach maximum along 58° W. This OBD has a well-defined origin near 11° N, 55.2° W in the FCDI analysis, which is about 0.6° latitude to the north and 1.2° longitude to the west of the OBD origin just three hours earlier (Figure 3a). The direct connection to a synoptic circulation to the north has also translated to about 1° longitude to the west. Similar to the AMV OBD in Figure 2b, there is a southwestward outflow branch from the northern outflow origin in the FCDI analysis that passes over the PTC 2 (black dot in Figure 3b), which would be expected to inhibit the intensification of the PTC 2. Note the alternating isotach maxima (>12 m s^{-1}) and minima (>9 m s^{-1}) along this northeasterly flow over the PTC 2, which may indicate gravity waves. Furthermore, there is now a direct connection of this southwestward OBD with the strong

(>21 m s^{-1}) northeasterly flow over the South American coast (indicated by a black line in Figure 3b).

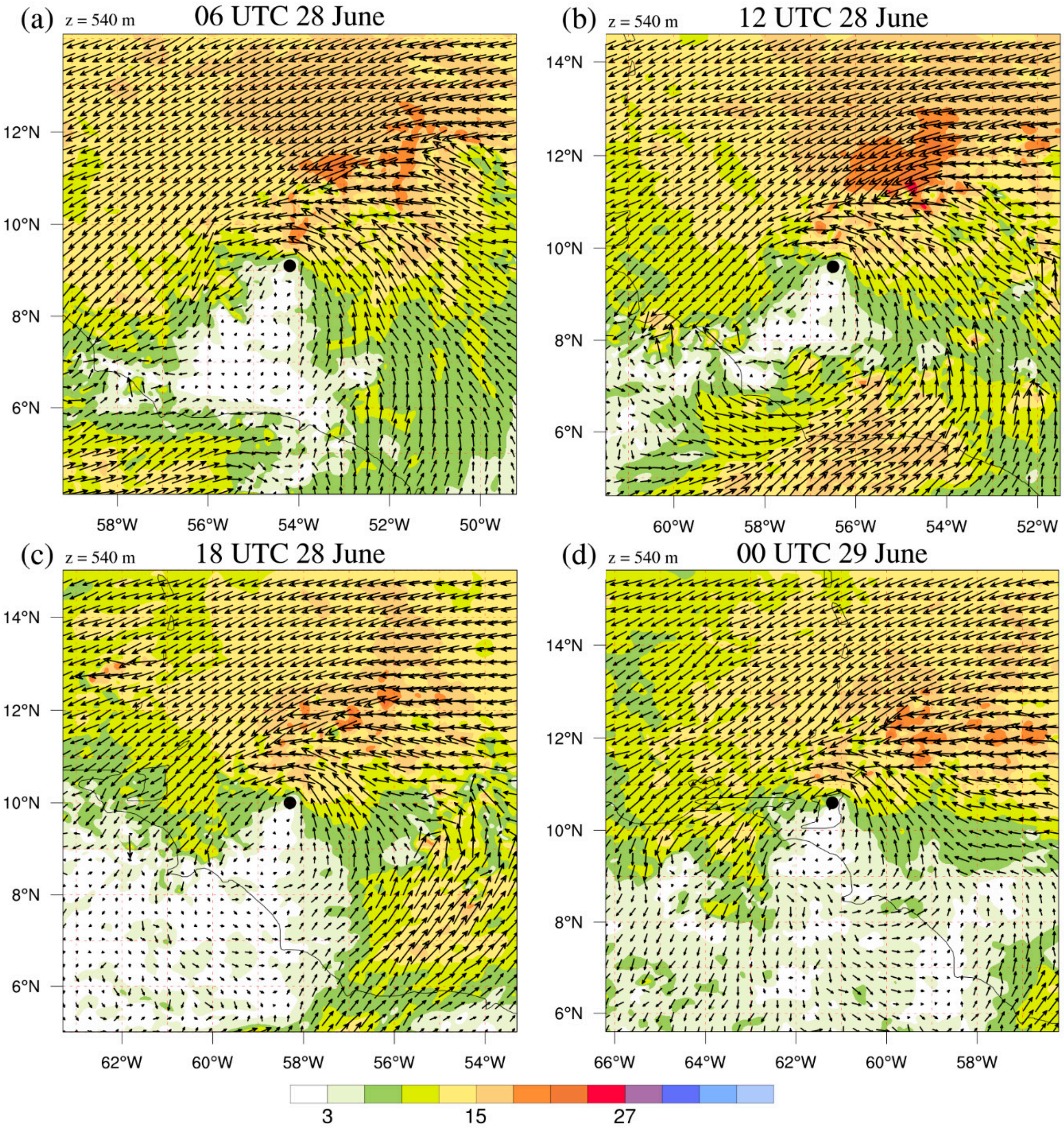

Figure 4. Wind vectors from continuous FCDI analyses as in Figure 3, except at 540 m for (**a**) 0600 UTC, (**b**) 1200 UTC, (**c**) and 1800 UTC 28 June, and (**d**) 0000 UTC 29 June.

The 0600 UTC 28 June FCDI wind vector analysis at 540 m (Figure 4a) is only 12 h after a cold-start initialization at 1800 UTC 27 June, in which a symmetric vortex was superposed on a background flow. Six hours later (not shown), small (<6 m s^{-1}) westerly winds still existed on the equatorward side of the PTC 2 vortex, which was more than 200 km north of the South American coast. After six more hours of AMV forcing, the FCDI analysis in Figure 4a represents the PTC 2 circulation as a southwest–northeast-tilted trough in the easterly flow that is connected to a vortex near 6.4° N, 58° W on the South American coast. The target six-hour PTC 2 center position of 9.0° N, 54.5° W from the 0600 UTC 28 June NHC Advisory that was used in the FCDI surface wind adjustment was successful in that the PTC 2 center in the continuous FCDI 540 m analysis was near 9.0° N, 54.2° W. In the discussion of the second AMV OBD near PTC 2 at 0900 UTC 28 June (Figure 2a), it was suggested that such an OBD might contribute to intensification of PTC 2 if the OBD was vertically aligned. *The key point is that the low-level circulation in* Figure 4*a does not wrap around the PTC 2 center in response to the heating in an OBD, because PTC 2 is analyzed as an open wave rather than a vortex.*

The FCDI 540 m wind analysis at 1200 UTC 28 June (Figure 4b) depicts an elliptical circulation that has two centers. The PTC 2 center is the northern center near 9.4° N, 56.8° W, which is a slight deviation from the NHC advisory position near 9.6° N, 56.5° W. The southern center in the elliptical circulation is near 7.8° N, 58.6° W, and is clearly related to the strong (>12 m s^{-1}) southwesterlies off the coast of South America. While wind speeds >18 m s^{-1} are analyzed to the north of the PTC 2 center, this is not the typical Tropical Storm structure. Rather, the elliptical circulation in Figure 4b more resembles a broad monsoon depression with equatorial westerlies (trade easterlies) on the south (north) side.

Recall that the AMV OBD at 1500 UTC (Figure 2c) had spread westward to ~60° W and had a southwestward branch that was west of the PTC 2. The 13,910 m FCDI OBD leading edge is also analyzed to be near 60° W (Figure 3c). This OBD origin is near 10.5° N, 57.2° W, which is just to the north of the PTC 2. Consequently, there are strong (>18 m s^{-1}) northeasterly wind vectors over the PTC 2 that would inhibit its intensification.

By 1800 UTC 28 June (Figure 2d), the northern AMV OBD had translated westward well beyond the PTC 2, and the long leading edge between 10° N, 58° W and 11.5° N, 58.5° W of a new OBD was approaching the PTC 2 (Figure 2d). The southern segment of the new OBD that is approaching PTC 2 is much weaker (~12 m s^{-1}) in the FCDI analysis (Figure 3d) than might have been inferred from the AMV OBD in Figure 2d. Since this new OBD had developed in the last three hours (compare Figure 2d with Figure 2c), the explanation may be that the FCDI analysis has not had time to respond.

The FCDI 540 m wind analysis at 1800 UTC 28 June (Figure 4c) occurred after the AMV datasets at 1500 UTC (Figure 2c) and 1800 UTC (Figure 2d) were assimilated into the FCDI analyses. The low-level PTC 2 circulation has propagated rapidly to the west so that it is no longer interacting with the southwesterlies coming off the coast of South America. The PTC 2 is now analyzed as a mesovortex near 10.0° N, 58.6° W that is embedded in northeasterlies in advance of the easterly wave trough. This PTC 2 position is consistent with the FCDI surface wind adjustment target position (10.1° N, 58.5° W). However, there is little evidence of an OBD above PTC 2 in the 13,910 m FCDI analysis at 1800 UTC 28 June (Figure 3d), as might have been expected with such a mesovortex with adjacent winds >21 m s^{-1}. Likewise, the AMV plot at 1800 UTC 28 June has no evidence of an OBD above the PTC 2. At 00 UTC 29 June (Figure 4d), the NHC position of PTC 2 is 10.6° N, 61.2° W, which then becomes the six-hour target position for the FCDI surface wind adjustment. By contrast, the FCDI-analyzed position (not indicated) is near 9.4° N, 59.4° W, which is attributed to the winds in advance of the PTC center having turned sharply to the south and having moved over Venezuela. In addition to slowing the westward translation of PTC 2, the intensity to the north of PTC 2 is about 15 m s^{-1} (Figure 4d).

In the case of PTC 2 during the 28 June, the long-lasting OBDs were mainly to the north and spread westward in a fan shape. It was only briefly and early on the 28 June that a short-lived OBD was centered near the PTC 2. Later on the 28 June, the southwestward flow from the dominant northern OBD swept over the PTC 2, which was not as favorable a condition for an RI event as would be hoped for a TCRI/HRD aircraft mission. It is not straight-forward to compare the FCDI-analyzed intensities with the constant 35 kt intensities (digitized to 5 kt intervals) in the NHC advisories, but the analyzed intensities were more within range of 35 kt rather than much higher wind speeds expected in an RI event.

3.2. June 29 AMV Datasets and FCDI Analyses

A second three-hourly sequence of GOES-16 AMVs relative to the PTC 2 from 0600 UTC 29 June to 1500 UTC 29 June is provided in Figure 5a–d. Already at 0600 UTC

(Figure 5a), a huge mature OBD exists over three-fourths of the GOES-16 mesodomain. The eastern half of the domain is shaded yellow, which means there are highly thinned AMVs above 100 mb that are dense enough to prevent visualization of the red (100–150 mb) AMVs. Where red AMVs are seen in the eastern half of the OBD, the divergence of those AMVs indicates other OBD centers (e.g., near 12° N, 62.6° W). In the western half of the OBD, the yellow AMVs thin out toward the leading edge and this reveals the red (100–150 mb) AMVs that extend to the leading edge. Note that PTC 2 is along the southern edge of this huge OBD.

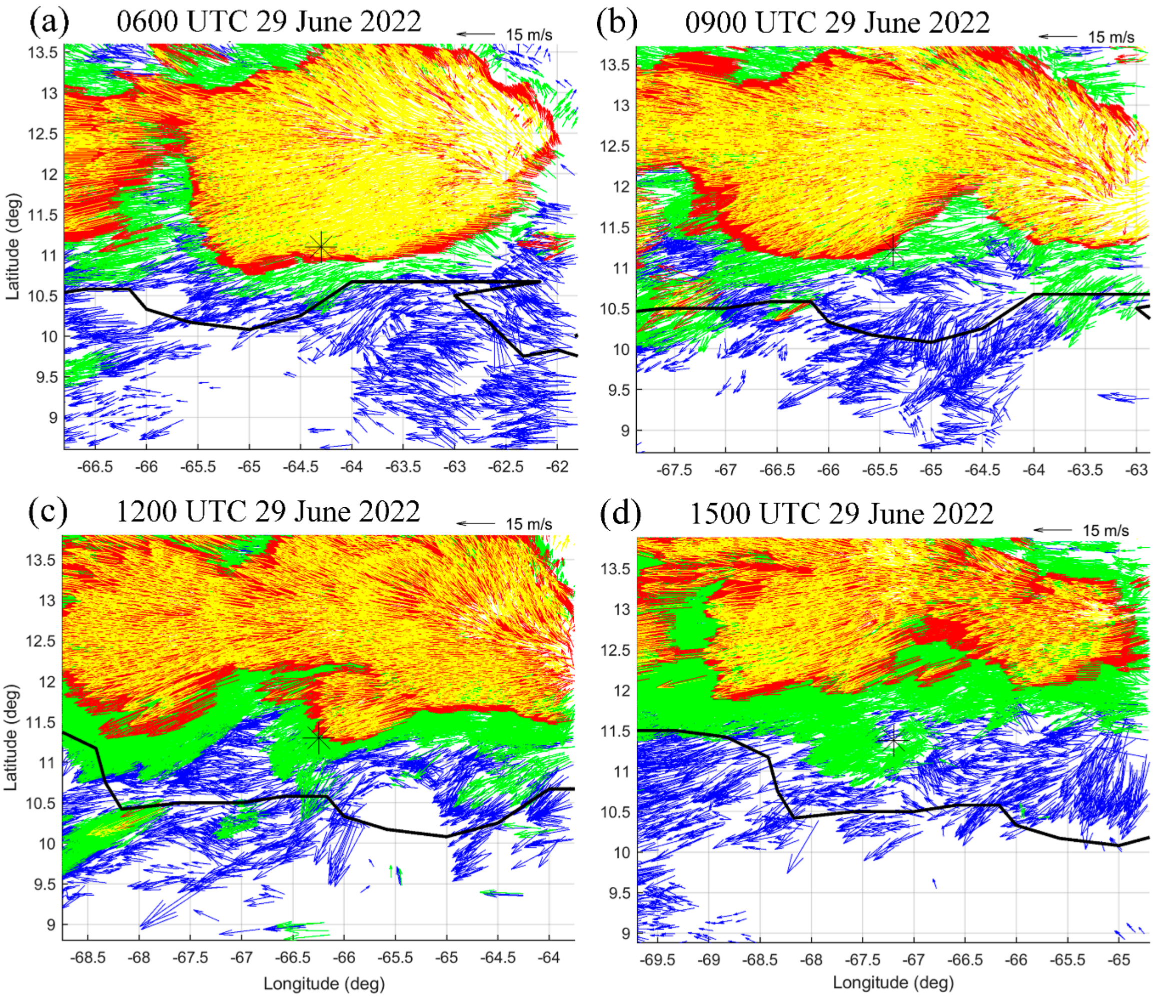

Figure 5. GOES-16 AMVs reprocessed at 15 min intervals with wind vector colors as in Figure 2, except centered on the near-surface positions of PTC 2 at (**a**) 0600 UTC 29 June, (**b**) 0900 UTC 29 June, (**c**) 1200 UTC 29 June, and (**d**) 1500 UTC 29 June.

In just three hours (Figure 5b), a new OBD exists with a center/origin near 11.8° N, 63.2° W. Although this new OBD has spread westward and northward, the strongest outflow is toward the northwest where it has overtaken and blended with the trailing edge of the huge OBD from 0600 UTC 29 June. Although the PTC 2 is translating rapidly to the west (Table 1, column 2), the huge OBD is spreading westward more rapidly. Consequently, the PTC 2 is on the southern trailing edge at an elevation of 150 mb (i.e., where red AMVs transition to green AMVs).

At 1200 UTC 29 June (Figure 5c), the huge OBD that existed at 0600 UTC 29 June has spread out even as it continued to move westward more rapidly than the PTC 2 translation speed. Meanwhile, a lobe of the new northwestward OBD has separated and approached the PTC 2 from the east–northeast. The PTC 2 continues to be on the leading edge of that lobe at an elevation of 150 mb according to the ending (beginning) of the red (green) AMVs. Note the broad width of the green (150–200 mb) AMVs all along the southern boundaries of the OBDs, which indicates that that layer has horizontally spread more rapidly to the south. Just three hours later (Figure 5d), the PTC 2 is now at the southern boundary of that "spread-out OBD", as the horizontal width of the green (150–200 mb) AMVs is even larger. In addition, the elevation of the highest (blue) AMVs above the PTC 2 is less than 200 mb, which would be consistent with a weak disturbance at 1500 UTC 29 June and beyond. Specifically, the opportunity for a TCRI/HRD aircraft mission at 18 UTC 29 June focused on an RI event associated with PTC 2 would not look favorable.

The continuous 13,910 m FCDI analysis at 06 UTC 29 June after 12 more hours of GOES-16 AMVs have been assimilated after the analysis in Figure 3d is provided in Figure 6a. This FCDI analysis clearly depicts the origin of the OBD near 12.0° N, 61.6° W and its westward-oriented fan shape. Note also the alternating blue (>30 m s^{-1}) isotach bands along that westward orientation, which are suggestive of gravity waves. Just as the PTC 2 was at the southern leading edge of the AMV OBD in Figure 5a, it is analyzed just inside the leading edge of the FCDI OBD in Figure 6a (black circle). Since the isotach in that region is >27 m s^{-1}, this is not a favorable upper-tropospheric environment for the development and intensification of PTC 2. Note also that the southwesterlies at 13,910 m over PTC 2 extend far inland over South America, which is the upper-tropospheric signature of the land–PTC 2 interaction.

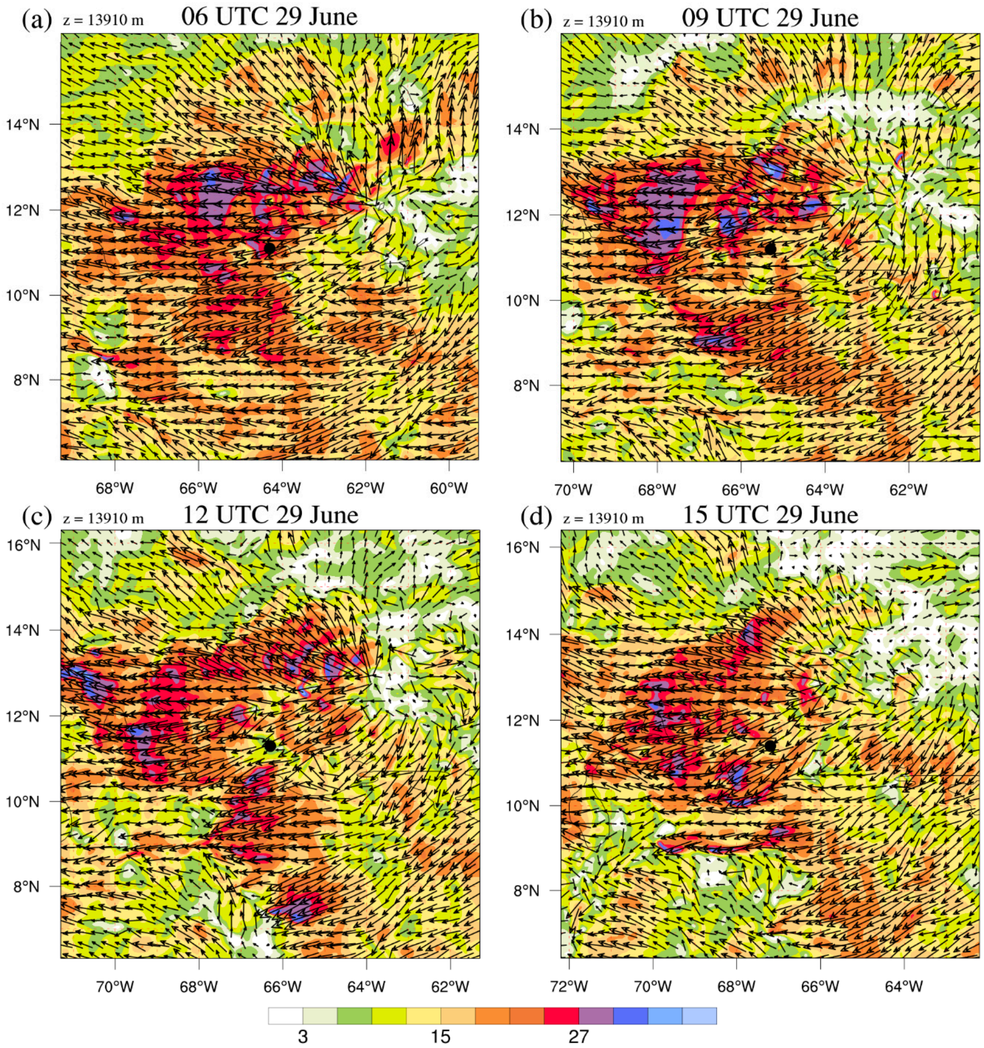

Figure 6. Wind vectors at 13,910 m from continuous FCDI analyses as in Figure 3, except for (**a**) 0600 UTC, (**b**) 0900 UTC, (**c**) 1200 UTC, and (**d**) 1500 UTC 29 June.

Recall from Figure 4d that the flow at z = 540 m in advance of PTC 2 had turned sharply toward the South American coast at 0000 UTC 29 June. This PTC 2–land interaction is even stronger at 0600 UTC (Figure 7a) as low-level northeasterlies in advance of PTC 2 penetrate far inland. Consequently, the low-level circulation of PTC 2 is poorly defined in the FCDI analysis, which is consistent with the unfavorable aloft environment, with >27 m s^{-1} wind speeds over PTC 2 at 13,910 m (Figure 6a).

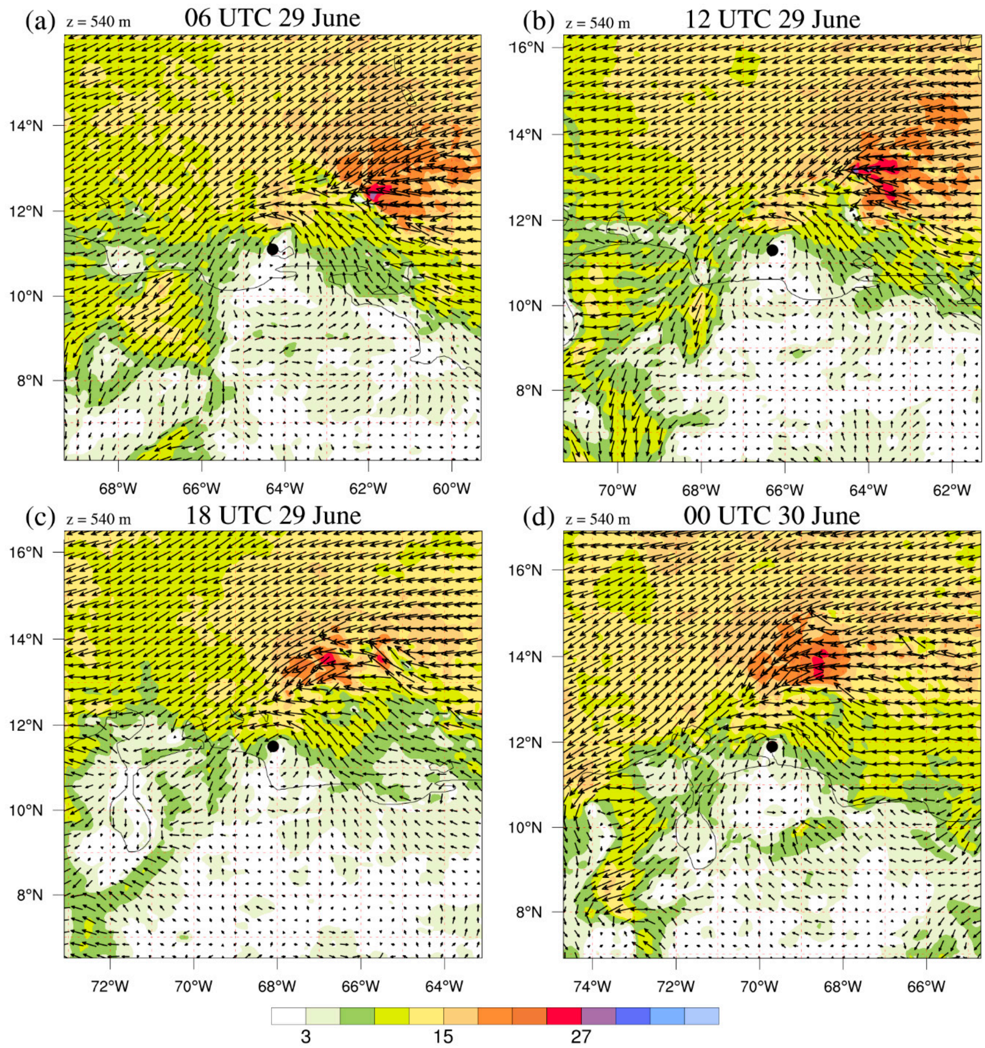

Figure 7. Wind vectors from continuous FCDI analyses as in Figure 3, except at 540 m for (**a**) 0600 UTC, (**b**) 1200 UTC, and (**c**) 1800 UTC 29 June, and (**d**) 0000 UTC 30 June.

The next continuous 13,910 m FCDI analysis at 0900 UTC 29 June in Figure 6b documents the new AMV OBD in Figure 5b that has a separate origin near 12° N, 63° W compared to the prior origin near 12° N, 62° W in Figure 6a. With this 1° longitude westward translation of the northern OBD, the PTC 2 is then on the trailing edge of the original northern AMV OBD in Figure 5b, and on the trailing edge of the FCDI OBD in Figure 6b. Thus, the upper-level flow over PTC 2 is reduced to less than 15 m s^{-1} at 0900 UTC 29 June (Figure 6b).

As was shown in Figure 5b, a lobe of high winds had broken off from the new AMV OBD and was encroaching on PTC 2. This sequence is displayed in the 13,910 m FCDI analysis at 1200 UTC (Figure 6c) with <12 m s^{-1} winds around PTC 2 and in a band to the north. Furthermore, an OBD leading edge is approaching from the east. While these rapid changes were evident at 0900 UTC and 1200 UTC in both the GOES-16 AMV dataset (Figure 5) and the 13,910 m analyses (Figure 6), the impact on the PTC 2 low-level flow

(Figure 7b) was as a mesovortex with weak winds (<3 m s^{-1}) near 10.8° N, 65.3° W. While an isotach maximum >15 m s^{-1} is analyzed just to the north of the PTC 2 center, the land interaction has opposed the development of PTC 2 at 1200 UTC 29 June.

Recall that, at 1500 UTC 29 June (Figure 5d), the AMV OBD was well to the north of PTC 2, which at that time was embedded within AMVs in the 150–200 mb layer. It is thus consistent that the continuous FCDI analysis at 13,910 m (Figure 6d) has PTC 2 in a region of <12 m s^{-1} isotachs. Although the NHC Advisory 8 at 1500 UTC 29 June has PTC 2 at 11.4° N, 67.3° W, the subsequent 540 m FCDI analysis (Figure 7c) has little evidence of circulation near that position. Rather, the onshore (offshore) flow ahead (behind) this target position indicates that the land interaction may have had a larger impact on PTC 2. Similarly, the 0000 UTC 30 June analysis at 540 m (Figure 7d) has very strong onshore flow between 71° W and 72° W over an inland gulf region of Venezuela.

In conclusion, the 29 June 15 min GOES-16 AMV dataset documents the persistence of the huge OBD from 28 June and the development and spreading of a new OBD. Between 0600 UTC (Figure 6a) and 0900 UTC (Figure 6b), the PTC 2 was along the southern leading edge of a lobe from the new OBD. One "bottom–up" inference from this GOES-16 dataset might be that the deep convection associated with PTC 2 was at least strong enough to limit the southern spreading of these two OBDs. An alternative, "top–down" inference would be that the vertical wind shear associated with these two OBDs was sufficiently large that it prevented the development and intensification of PTC 2.

The continuous 13,910 m FCDI analyses at 0600 UTC (Figure 6a), 0900 UTC (Figure 6b), and 12 UTC 29 June (Figure 6c) tend to support the bottom–up inference. Each of these 13,910 m analyses document that there was also strong northeasterly flow over northern South America. In each of these three FCDI analyses, the existence of the PTC 2 outflow interfered with a direct connection between the northern Caribbean OBDs and the upper-tropospheric northeasterly flow over northern South America. In Figure 6a, PTC 2 is analyzed at 13,910 m to be just within the leading edge of the OBD; but, in Figure 6b,c, the outflow above PTC 2 appears to deflect and/or oppose the encroaching northeasterlies associated with the northern OBDs. Thus, the FCDI analyses suggest a two-way interaction, since the environmental vertical wind shear is also inhibiting development during 29 June.

The continuous 540 m FCDI analyses in Figure 7a–c document the fact that the interaction of the PTC 2 low-level flow with the adjacent land was a strong contributing factor in its lack of development during 29 June. At 0600 UTC when PTC 2 was just inside the OBD leading edge (Figure 5a), the low-level northeasterlies associated with PTC 2 were crossing the coast and joining with northeasterlies farther inland (Figure 7a). Thus, both vertical wind shear associated with the OBD and frictional effects due to the land likely inhibited PTC 2 development at 0600 UTC 29 June. Similarly, land interaction at 1200 UTC (Figure 7b) and 1800 UTC (Figure 7c) with northeasterlies crossing the coast, rather than wrapping around the equatorial side of PTC 2, were not favorable for development. Finally, the northeasterly onshore flow >12 m s^{-1} between 71° W and 72° W at 00 UTC 30 June (Figure 7d) was totally inconsistent with development of PTC 2, which at that time NHC had the position at 11.9° N, 69.7° W.

Based on these continuous FCDI analyses, PTC 2 during 29 June was definitely not an appropriate target for a TCRI/HRD aircraft mission to obtain observations in an RI event. NHC had continued to advise that PTC 2 had a constant intensity of 35 kt rather than being a Tropical Storm. These 540 m FCDI analyses during 29 June confirm the presence of very small westerly winds, but do not necessarily confirm constant near-surface 35 kt winds on the south side, and thus might be considered a TC. However, these analyses do not necessarily confirm constant near-surface 35 kt winds in the vicinity of the NHC advisory center positions. In answer to the "why not" question, the PTC 2 outflow interactions with the OBDs to the north likely contributed, but the primary reason was the interaction of the PTC 2 low-level circulation with land, as depicted in Figure 7.

4. Could PTC 2 Have Become a Caribbean False Alarm Circulation?

Elsberry et al. [6] examined four categories of Atlantic TC events (formations plus tracks) predicted by the 32-day ECEPS during the 2012 season. Because not a single southern Caribbean disturbance developed into a Tropical Storm, those disturbances were considered to be false alarms (FAs) as far as Atlantic TC formation events were concerned. Capalbo (2022) [17] and Elsberry et al. [3,18] documented that, during the 2021 eastern North Pacific season, the 15-day ECEPS predicted questionable ensemble storms that would start very near the west coast of Central America and move to the northwest parallel to the coast. Except for some forecasts in which the ensemble storms made landfall or strongly interacted with land, the ECEPS was predicting that the storms would intensify to the hurricane stage, including an RI event immediately following formation [17,18].

An example from Elsberry et al. [18] of an ECEPS FA forecast that included ensemble member tracks extending back to the southern Caribbean is shown in Figure 8. In that 0000 UTC 14 August 2021 ECEPS forecast, Storm 26 had a maximum of 13 member tracks, and 10 of these member tracks had started in or crossed into the eastern North Pacific. Note that the WMVM track (red dots) originated at 0000 UTC 14 August with three members in the southern Caribbean Sea. Even though there are more ensemble member storms that later form in the eastern North Pacific, the WMVM track forecast technique would give those storms little weight compared to those tracks within an eastern cluster of tracks that are so much closer to the WMVM track.

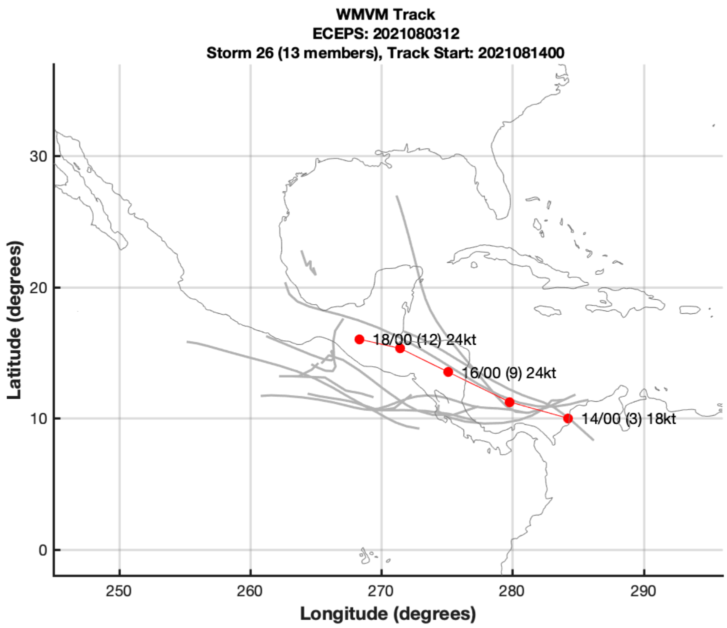

Figure 8. Weighted Mean Vector Motion (WMVM, red line) track forecast similar to Figure 1 that started at 0000 UTC 14 August 2021 from three member tracks on or near the Venezuelan coast.

Elsberry et al. (Section 2 in [18]) describe their efforts to accurately identify those FA ensemble storm tracks in the southern Caribbean. When those efforts failed, the solution was to exclude all ensemble member tracks that crossed Central America into, or originated within, a small box (8° N–13° N; western boundary at 93° W) in the eastern Pacific. This solution then limits the early detection of TC formations to those that start west of 93° W. While it was shown by Elsberry et al. [18] to successfully exclude nearly all FA storms in eastern North Pacific during the 2021 season, it also excludes real storms in the western Caribbean that do cross Central America and may become a Tropical Storm or Hurricane close to the coast. For example, storms such as the southern Cluster 1 track or the middle Cluster 2 track in Figure 1 would not be considered as a potential Hurricane Bonnie in the eastern North Pacific until after crossing 93° W. Thus, it would be very helpful to identify and predict which southern Caribbean disturbances will, or will not, be FAs when they are passing close to the Venezuelan coast.

The question, then, is whether a regional numerical model could better predict whether PTC 2 would have not undergone RI while passing along the Venezuelan coast, but actually had characteristics of an FA until 0000 UTC 1 July. As demonstrated in Elsberry et al. [7], the FCDI analyses can also be utilized as the initial conditions for the COAMPS-TC forecast model. Because the same model is being utilized in the dynamic initialization, the forecasts start off smoothly without any dynamic or thermodynamic re-balancing required. It is noted that the COAMPS version used here as the Control is the same COAMPS version utilized in the cold-start of the FCDI analyses. Whereas that cold-start FCDI analysis included a bogus vortex based on the TC Vitals, after that initial FCDI analysis at 1800 UTC 27 June, no bogus vortex has been included. By contrast, each of our Control COAMPS-TC forecasts without the GOES-16 AMV datasets does begin with a bogus vortex (note: operational COAMPS-TC does not utilize a bogus vortex until 55 kt).

Comparisons of the COAMPS-TC Forecast-1 and Forecast-2 track forecasts with the Control COAMPS-TC track forecasts from the same initial times are provided in Table 2. Deviations of these track forecasts are calculated relative to the PTC 2 positions in the continuous FCDI analyses to document the impact of the GOES-16 AMV datasets added in the FCDI analyses. Note that the Control-1 track forecast (Table 2, column 3) from 0000 UTC 28 June immediately took a >1°-latitude farther south track than the FCDI analyses, with a maximum deviation of −1.7° latitude at 0000 UTC 30 June. Consequently, the Control-1 track was mostly over land, which likely contributed to the large negative longitude deviations (maximum of −3.8° longitude) relative to the FCDI analyses. Interestingly, the COAMPS-TC Forecast-1 (Table 2, column 4) also has southward track deviations, with a maximum of −1.3° latitude. The COAMPS-TC track Forecast-1, then, also has slow along-track biases, especially at 0000 UTC 1 July, where PTC 2 was mistakenly located at 10.2° N, 74.1° W (see Figure 9 and discussion below).

Table 2. Control track Forecast-1 (column 3) versus COAMPS-TC track Forecast-1 (column 4) initialized from 0000 UTC 28 June with deviations from the continuous FCDI analysis track positions in column 2 indicated within parentheses on the row below. Control Forecast-2 (column 5) and COAMPS-TC Forecast-2 (column 6) initialized from 1200 UTC 28 June also compared with the continuous FCDI analyzed track positions.

Time	FCDI	CONTROL-1	FORECAST-1	CONTROL-2	FORECAST-2
00UTC 6/28	8.5° N, 52.0° W	8.4.° N, 52.0° W (−0.1; 0.0)	8.5° N, 52.0° W (0.0; 0.0)		
12 UTC 6/28	9.6° N, 56.4° W	8.5° N, 55.5° W (−1.1; −0.9)	8.8° N, 55.1° W (−0.8; −1.3)	7.5° N, 56.2° W (−2.1; −1.3)	9.5° N, 56.5° W (−0.1; +0.1)
00 UTC 6/29	10.4° N, 61.2° W	8.8° N,59.6° W (−1.6; −1.6)	9.5° N, 59.5° W (−0.9; −1.7)	10.6° N, 59.2° W (+0.2; −1.7)	10.1° N, 59.4° W (−0.3; −1.8)
12 UTC 6/29	11.5° N, 66.2° W	10.0° N, 62.6° W (−1.5; −3.6)	10.2° N, 63.9° W (−1.3; −2.3)	12.1° N, 65.8° W (+0.6; −0.4)	10.5° N, 64.7° W (−1.0; −1.5)
00 UTC 6/30	11.8° N, 69.8° W	10.1° N, 66.0° W (−1.7; −3.8)	10.6° N, 68.8° W (−1.2; −1.0)	12.3° N, 69.8° W (+0.5; 0.0)	11.6° N, 69.6° W (−0.2; −0.2)
12 UTC 6/30	11.2° N, 73.8° W	10.0° N, 76.6° W (−1.2; +2.8)	10.3° N, 71.8° W (−0.9; −2.0)	12.6° N, 74.6° W (+1.4; +0.8)	11.5° N, 73.8° W (+0.3; +0.0)
00 UTC 7/1	11.2° N, 77.2° W	11.0° N, 74.5° W (−0.2; −2.7)	10.2° N, 74.1° W (−1.0; −3.1)	12.5° N, 78.8° W (+1.3; +1.6)	11.0° N, 78.0° W (−0.2; +0.8)

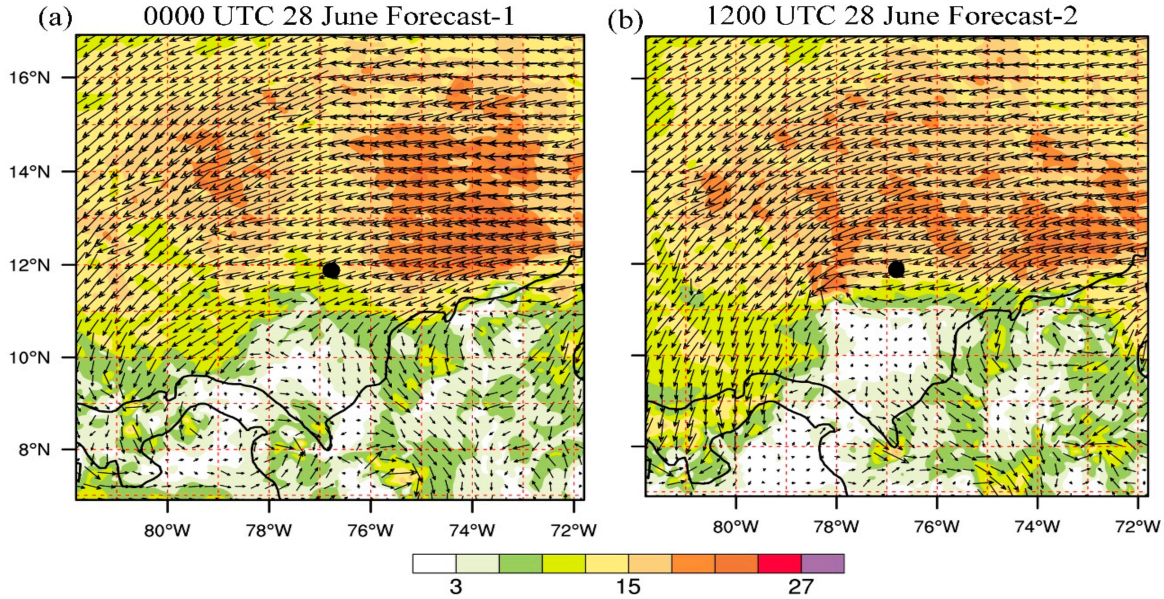

Figure 9. Wind vectors at 540 m at 0000 UTC 1 July from COAMPS-TC forecasts initialized from the continuous FCDI analysis at (**a**) 0000 UTC 28 June and at (**b**) 1200 UTC 28 June.

The initial position in the Control-2 forecast (Table 2, column 5) was poorly defined at 7.5° N, 56.2° W, which is 2.1° latitude to the south and 1.3° longitude to the east of the FCDI position at 1200 UTC 28 June. However, the Control-2 track forecast quickly adjusted to a westward path at higher latitudes, with deviations that were as large as 1.4° latitude at 1200 UTC 30 June. With a path farther to the north, the westward translation speeds were greater and the initial eastward track deviations relative to the FCDI analysis positions were changed to northwestward track deviations. Nevertheless, the Control-2 track forecast was reasonable considering how rapidly the PTC 2 disturbance was translating (Table 1, column 2).

The COAMPS-TC track Forecast-2 (Table 2, column 6) demonstrates the positive impacts of assimilating the GOES-16 AMV datasets well. Except for one forecast at 1200 UTC 29 June, the latitude deviations relative to the FCDI analysis positions are within +/−0.3° latitude. With these almost perfect track latitudes with respect to the Venezuelan coast, the longitude deviations (Table 2, column 6) are better than in the Control-2 forecast, especially during the last three forecasts. One exception of a too-slow westward translation of −1.5° longitude occurred when the latitude deviation was −1.0°, which means the PTC 2 was predicted to be inland.

Although this demonstration is for only two forecasts, the FCDI analyses including the GOES-16 AMV datasets can provide improved track forecasts in a difficult case of a PTC 2 strongly interacting with land and therefore not undergoing RI.

In addition to predicting the non-RI due to land interaction as PTC 2 passed along the Venezuelan coast, the COAMPS-TC must also predict the NHC track and intensity (constant 35 kt until 0000 UTC 1 July—Table 1) evolution after PTC 2 moves over open ocean. The 540 m wind field at 0000 UTC 1 July from the 0000 UTC 28 June COAMPS-TC Forecast-1 indicates a weak wave in the easterlies with the apex of the wave about 100 km to the south–southwest of the NHC best-track position (black dot, Figure 9a). Moreover, a large cyclonic circulation centered near 10° N, 74° W is also predicted. This position is relatively close to the 0000 UTC 14 August position for the FA circulation in Figure 8, which raises the question as to whether this cyclonic circulation, induced by the passage of PTC 2, could later become an FA circulation. In the 1200 UTC 28 June Forecast-2 (Figure 9b), the PTC 2 is represented as a short-wave trough near 11.2° N, 78.0° W. By contrast, the PTC 2 best-track position near 11.8° N, 76.8° W has a triangular-shaped isotach maximum exceeding 24 m s^{-1} in the northern semicircle that is more representative of a wave in the easterlies. As in Forecast-1 in Figure 9a, a large cyclonic circulation centered near 10.6° N, 74.0° W is predicted in the COAMPS-TC Forecast-2, which again may become an FA circulation since the position along the coast is so similar to the FA position in Figure 8. An objective of future research will be to examine subsequent ECEPS forecasts after 0000 UTC 1 July to determine whether this cyclonic circulation did become a Caribbean FA in the eastern North Pacific.

5. Summary and Discussion

The Elsberry et al. [3] ECEPS-based tropical cyclone lifecycle prediction of PTC 2 from 0000 UTC 24 June has been utilized to provide early guidance as to whether PTC 2 would undergo RI as it passed along the coast of Venezuela, and thus whether it would have provided an opportunity for a TCRI aircraft mission. The predicted track spread about the WMVM track was relatively small until PTC 2 passed Venezuela, but then a track trifurcation of three track clusters was predicted among the 50 ECEPS members. While the middle and northern track clusters both had two RI events associated with them, the southern track cluster, which ultimately best represented the path that PTC 2 took, did not have an associated RI event. Indeed, the intensity predictions along the southern track from 0000 UTC 28 June (Day 4) to 0000 UTC 1 July were quite close to the constant 35 kt intensities in the NHC advisories during that period.

The primary question then was the following: what physical processes led to these near-constant intensities during 28 June and 29 June when PTC 2 was passing north of Venezuela? The continuous (15 min) FCDI analyses starting from 1800 UTC 27 June demonstrate the need for, and the advantages of, utilizing the CIMSS-reprocessed 15 min GOES-16 AMV datasets in the continuous FCDI analyses. Those GOES-16 AMVs reveal long-lasting outflow bursts extending above 100 mb that rapidly spread out over hundreds of kilometers, which were helpful in visualizing potential opportunities for RI events. Only the mesodomain AMVs are capable of depicting the source regions and rapid spreading of the OBDs, including the leading edge, where rapid descent occurred over short distances. Indeed, TC forecast centers might consider video loops of these 15 min AMV datasets as a supplement to the operational geostationary satellite visible and infrared loops.

It is noteworthy in this PTC 2 example that the continuous FCDI analysis technique has been capable of assimilating more than 10,000 AMVs (recall that only one in ten AMVs were shown above) that the CIMSS had reprocessed each 15 min. Consequently, the continuous FCDI analyses at 13,910 m in Figures 3 and 6 represented well the long-lasting outflow bursts to the north of PTC 2. Another special advantage of these FCDI analyses with the surface wind adjustment is that they represented the westward propagation of the PTC 2 well. Because the PTC 2 was moving westward so rapidly, assimilation of just hourly AMVs would not have been able to accurately resolve these interactions of the PTC 2 with the adjacent land that likely inhibited the development of the PTC 2.

Diagnosis of the low-level wind speeds in PTC 2 is possible from the continuous FCDI analyses because the COAMPS model integration nudges the interior three-dimensional wind, pressure, and humidity fields to the 15 min GOES-16 AMV datasets. The 1200 UTC 28 June to 0000 UTC 29 June FCDI 540 m wind analyses in Figure 4b–d document that the PTC2 northerly winds do not wrap around the center in response to diabatic heating in the column. Rather, the northeasterly flow in advance of the center extends to the coastline, and strong southwesterly flow is pulled offshore behind PTC 2. The FCDI 540 m wind analyses in Figure 4 document the strong land interaction as the PTC 2 center is just offshore. While there are some 540 m wind speeds of ~15 m s^{-1} to the north of the center, only weak winds are diagnosed to the south of the center. Thus, the land interaction with the PTC 2 circulation is the explanation for the constant 35 kt intensities in the NHC advisories.

While the primary objective has been to demonstrate that continuous FCDI analyses can be utilized with the GOES-16 AMV datasets to diagnose the PTC 2 track and intensity, we also demonstrate the FCDI analyses can be utilized as initial conditions for COAMPS-TC forecasts of PTC 2. Comparisons with control forecasts in Table 2 document the better tracks and intensities from assimilating the GOES-16 AMV datasets in the FCDI analyses. The two COAMPS forecasts (Table 2) that utilize the FCDI analyses initial conditions also successfully predict a cyclonic circulation farther westward down the coast that may become a false alarm circulation both in the southern Caribbean and in the eastern North Pacific.

Author Contributions: R.L.E. and C.S.V. together published journal articles utilizing the high-density Atmospheric Motion Vector (AMV) datasets. R.L.E. and H.-C.T. together published journal articles since 2014 on the ensemble storm Weighted Mean Vector Motion (WMVM) methodology. C.S.V. and his CIMSS AMV team provided the AMV files for J.W.F. to develop the outflow burst domes (OBDs) that are key to describing the non-rapid intensification of pre-Bonnie. H.-J.C. performed the computer coding and prepared the continuous FCDI analyses every 15 min. Interpretation: R.L.E. was the primary analyst. Writing: R.L.E. was responsible for the text. J.W.F., H.-C.T. and H.-J.C. were responsible for creating the figures. All authors have read and agreed to the published version of the manuscript.

Funding: R.L.E. is funded by Office of Naval Research Project N0001429280 and J.W.F. and H.J.C. are funded by N0001421WX00579. H.C.T. is supported by the Taiwan National Science and Technology Council (NSTC 112-2625-M-032-001).

Institutional Review Board Statement: Not applicable.

Informed Consent Statement: Not applicable.

Data Availability Statement: The GOES-16 AMV datasets processed during PTC 2 are available from CIMSS upon request (dave.stettner@ssec.wisc.edu). The ECMWF ensemble forecasts for the PTC 2 period are generally open only to member countries, or to affiliated countries with data-sharing agreements.

Conflicts of Interest: The authors declare no conflicts of interest. The funders had no role in the design of the study. The analyses or interpretation of the data, in the writing of the manuscript, or in the decision to publish the results.

References

1. Rios-Berrios, R.; Finocchio, P.M.; Allard, J.J.; Chen, X.; Fischer, M.S.; Stevenson, S.N.; Tao, D. A review of the interactions between tropical cyclones and environmental vertical wind shear. *J. Atmos. Sci.* **2024**, *84*. [CrossRef]
2. Papin, P.P. National Hurricane Center Tropical Cyclone Report, Hurricane Bonnie AL022022. NOAA/National Hurricane Center. 2023; 25p. Available online: www.nhc.noaa.gov/data/tcr/AL022022_EP042022_Bonnie.pdf (accessed on 10 January 2024).
3. Elsberry, R.L.; Tsai, H.-C.; Capalbo, C.; Chin, W.-C.; Marchok, T.P. Opportunity for tropical cyclone lifecycle predictions from pre-formation to ending stage: Eastern North Pacific 2021 season. *Atmosphere* **2022**, *13*, 1008. [CrossRef]
4. Marchok, T. Important factors in tracking of tropical cyclones in operational models. *J. Appl. Meteor. Climatol.* **2021**, *60*, 1265–1284. [CrossRef]
5. Doyle, J.D.; Hodur, R.M.; Chen, S.; Jin, Y.; Moskaitis, J.R.; Wang, S.; Hendricks, E.A.; Jin, H.; Smith, T.A. Tropical cyclone prediction using COAMPS-TC. *Oceanography* **2014**, *21*, 104–115. [CrossRef]
6. Elsberry, R.L.; Tsai, H.-C.; Jordan, M.S. Extended-range forecasts of Atlantic tropical cyclone events during 2012 using the ECMWF 32-day ensemble predictions. *Weather Forecast.* **2014**, *29*, 271–288. [CrossRef]
7. Elsberry, R.L.; Feldmeier, J.W.; Chen, H.-J.; Peng, M.; Velden, C.S.; Wang, Q. Challenges and opportunities with new generation geostationary meteorological satellite data sets for analyses and initial conditions for forecasting Hurricane Irma (2017) rapid intensification event. *Atmosphere* **2020**, *11*, 1200. [CrossRef]
8. Stettner, D.; Velden, C.S.; Rabin, R.; Wanzong, S.; Daniels, J.; Breskey, W. Development of enhanced vortex scale atmospheric motion vectors for hurricane applications. *Remote Sens.* **2019**, *11*, 1981. [CrossRef]
9. Elsberry, R.L.; Buholzer, N.; Velden, C.S.; Jordan, M.S. Satellite-based observations of nonlinear relationships between vertical wind shear and intensity changes during the lifecycle of Hurricane Joaquin (2015). *Weather Forecast.* **2020**, *35*, 939–959. [CrossRef]
10. Berg, R.L. Hurricane Joaquin (28 September–7 October 2015). National Hurricane Center Tropical Cyclone Report AL112015. 2016; 36p. Available online: www.nhc.noaa.gov/data/tcr/AL112015_Joaquin.pdf (accessed on 10 January 2024).
11. Hendricks, E.A.; Elsberry, R.L.; Velden, C.S.; Jorgensen, A.; Jordan, M.S.; Creasey, R. Environmental factors and internal processes contributing to interrupted rapid decay of Hurricane Joaquin (2015). *Weather Forecast.* **2018**, *33*, 1251–1262. [CrossRef]
12. Velden, C.S.; Herndon, D. A consensus approach for estimating tropical cyclone intensity from meteorological satellites: SATCON. *Weather Forecast.* **2020**, *35*, 1645–1662. [CrossRef]

13. Cangialosi, J.P.; Letto, A.S.; Berry, R. National Hurricane Center Tropical Cyclone Report, Hurricane Irma AL110217. NOAA/National Hurricane Center. 2018; 111p. Available online: www.nhc.noaa.gov/data/tcr/AL112017_Irma.pdf (accessed on 10 January 2024).
14. Lewis, W.E.; Velden, C.S.; Stettner, D. Strategies for assimilating high-density atmospheric motion vectors into a regional tropical cyclone forecast model (HWRF). *Atmosphere* **2020**, *11*, 673. [CrossRef]
15. Elsberry, R.L.; Feldmeier, J.W.; Chen, H.-J.; Velden, C.S. High temporal resolution analyses with GOES-16 atmospheric motion vectors of mesovortex rapid intensification in subtropical cyclone Henri (2015). *Weather Forecast.* **2023**, *38*, 1173–1194. [CrossRef]
16. Pasch, R.J.; Berg, R.; Hagen, A.B. Hurricane Henri (AL082021), National Hurricane Center Tropical Cyclone Report. 2022. Available online: www.nhc.noaa.gov/data/tcr/AL082021_Henri.pdf (accessed on 10 January 2024).
17. Capalbo, C.A. Application of Tropical Cyclone Lifecycle Predictions from Pre-Formation Stages: Eastern North Pacific 2021 Season. Master's Thesis, Naval Postgraduate School, Monterey, CA, USA, 2022; 108p.
18. Elsberry, R.L.; Tsai, H.-C.; Capalbo, C.; Chin, W.-C.; Marchok, T. Critical pre-formation decision flowchart to apply tropical cyclone lifecycle predictions in eastern North Pacific. *Atmosphere* **2023**, *14*, 616. [CrossRef]